Turbulent Fluctuations with an Electron Gyro-Scale in the National Spherical Torus Experiment

E. Mazzucato,[1,*] **D. R. Smith**,[1] **R. E. Bell**,[1] **J. C. Hosea**,[1] **S. M. Kaye**,[1] **B. P. LeBlanc**,[1] **P. M. Ryan**,[2] **J. R. Wilson**,[1] **H. Yuh**[3] **and the NSTX Group**

[1]Princeton Plasma Physics Laboratory, Princeton University, Princeton, New Jersey 08543, USA
[2]Oak Ridge National Laboratory, Oak Ridge, Tennessee 37831, USA
[3]Nova Photonics Inc., Princeton, NJ 08540, USA

*E-mail: mazzucato@pppl.gov

Abstract

Various theories and numerical simulations support the conjecture that the ubiquitous problem of anomalous electron transport in tokamaks may arise from a turbulence driven by the electron temperature gradient. To check whether this turbulence is present in plasmas of the National Spherical Torus Experiment (NSTX), measurements of turbulent fluctuations were performed with coherent scattering of electromagnetic waves. Results from plasmas heated by high harmonic fast waves (HHFW) show the existence of density fluctuations in the range of wave numbers $k_\perp \rho_e$=0.1-0.4, corresponding to a turbulence scale length of the order of the collisionless skin depth. Experimental observations and agreement with numerical results from a linear gyrokinetic stability code indicate that the observed turbulence is driven by the electron temperature gradient. Finally, turbulent fluctuations were not observed at the location of an internal transport barrier driven by a strong negative magnetic shear.

PACS numbers: 52.55.Fa, 52.35.Qz, 52.35.Ra

---

1. Introduction

Understanding the mechanism of plasma transport in tokamaks is one of the great challenges of fusion research. Indeed, since most explanations of this phenomenon are based on some type of turbulence [1-3], understanding plasma transport is tantamount to understanding turbulence. Unfortunately, since this is a tremendously difficult problem, the cause of anomalous energy losses in tokamaks is still an outstanding issue.

Particularly difficult to explain is the transport of electron energy. This is the most worrisome since in a tokamak reactor a large fraction of the energy of charged fusion products – necessary to sustain the nuclear fusion reactions – would be released directly to the electrons. Various theories and numerical simulations [4–9] support the conjecture that anomalous electron transport may arise from a turbulence driven by the Electron Temperature Gradient (ETG) instability. However, even though a limited circumstantial evidence has been presented in [10] on the role of an ETG turbulence on electron transport in Tore Supra, and measurements on FT-2 of fluctuations with an electron gyro-scale have been reported in [11], the existence in tokamaks of a turbulence driven by the electron temperature gradient has never been proved experimentally.

To investigate this type of turbulence, a series of experiments have been performed in plasmas of the National Spherical Torus Experiment (NSTX). These plasmas are uniquely suited for the

study of the physics of electron transport since, while the confinement of ions in NSTX is very often at or near neoclassical levels, that of electrons is anomalous in all operational regimes [12]. Preliminary results from these experiments have been presented in [13]. Here, we give a more detailed description of our measurements of short scale turbulent fluctuations driven by the electron temperature gradient in NSTX plasmas.

2. Coherent scattering of electromagnetic waves

Short-scale density fluctuations were measured with coherent scattering of electromagnetic waves, a powerful technique that was used extensively in early studies of plasma turbulence, including the first detection of short-scale turbulence in tokamaks [14]. The process can be characterized by an effective differential cross section per unit volume

$$\sigma = r_0^2 S(\boldsymbol{k},\omega) \ , \qquad (1)$$

where $r_0 = e^2/mc^2$ is the classical radius of electrons and $S(\boldsymbol{k},\omega)$ is the spectral density of fluctuations [15]. The mean square density fluctuation is obtained from

$$\langle\, |\tilde{n}_e|^2 \,\rangle = \frac{1}{(2\pi)^4} \int S(k,\omega)\, dk\, d\omega . \qquad (2)$$

Frequency (ω) and wave vector ($\boldsymbol{k}$) of fluctuations must satisfy the energy and momentum conservation

$$\omega = \omega_s - \omega_i , \quad \boldsymbol{k} = \boldsymbol{k}_s - \boldsymbol{k}_i , \qquad (3)$$

where superscripts s and i refer to scattered and incident waves, respectively. Since for the topic of this paper $\omega_s \approx \omega_i$ and $k_s \approx k_i$, the scattering angle θ must satisfy the Bragg condition $k = 2k_i \sin(\theta/2)$.

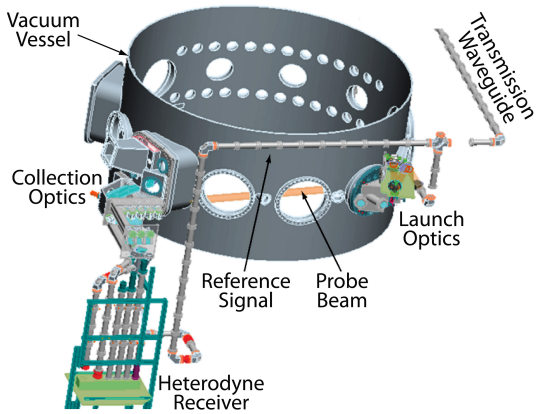

Figure 1. *Schematic illustration of the scattering apparatus showing some major hardware components.*

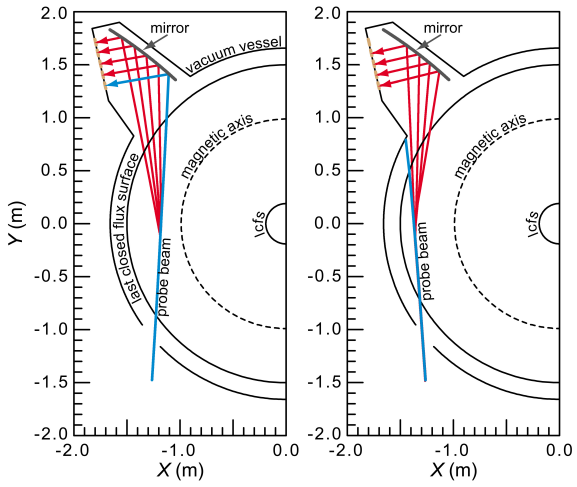

Figure 2. *Probe beam (blue) and scattered waves (red) for detection of inboard (left) and outboard (right) fluctuations. Steerable optics can position*

The NSTX scattering system (figure 1) employs a probing wave with a frequency of 280 GHz, together with a five-channel heterodyne receiver capable of providing full information on the frequency spectrum of measured signals [16]. A unique feature of the scattering geometry is an oblique propagation of the probing beam with respect to the magnetic field with both probe and scattered waves lying nearly on the equatorial midplane (figure 2), so that the wave vectors of measured fluctuations are nearly perpendicular to the magnetic surfaces. However, they have also small components in both

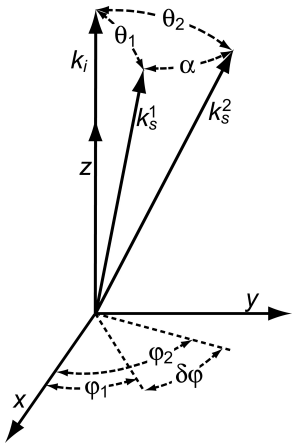

***Figure 3**. Orthogonal coordinates (x,y,z) with the z-axis along the wave vector of probing beam.*

diamagnetic and toroidal directions, from which one can infer the phase velocity of fluctuations in the poloidal plane.

The instrumental resolution of scattering measurements is limited by the size of probing and scattered beams, both having a Gaussian profile with a radius (a) of 2.5 cm in the present experiment. If we take the size of the common region to the two beams as a measure of spatial resolution (δl), we get $\delta l = 4k_i a/k$, that in our case gives δl=60 cm for k=10 cm^{-1}. From this, we might conclude that it is difficult to perform localized measurements of plasma turbulence with coherent scattering of electromagnetic waves. Fortunately, this estimate is valid only for an isotropic turbulence – which is not the case in tokamak plasmas where short-scale fluctuations satisfy the relation $\boldsymbol{k}\cdot\boldsymbol{B}/B \approx 1/qR$ [1,2] (with $\boldsymbol{B}$ the magnetic field, q the magnetic safety factor and R the plasma major radius). For all practical purposes, then, we can assume

$$\boldsymbol{k}\cdot\boldsymbol{B} \approx 0, \tag{4}$$

that, because of the large curvature of magnetic field lines, makes the instrumental selectivity function, i.e., the collection efficiency of scattered waves, strongly localized [17, 18]. This can be seen by considering the scattered waves originating from two points of the probing beam with wave vectors $\boldsymbol{k}_s^1$ and $\boldsymbol{k}_s^2$. From figure 3, we get

$$\frac{\boldsymbol{k}_s^1\cdot\boldsymbol{k}_s^2}{k_i^2} \equiv \cos\alpha = \cos\theta_1\cos\theta_2 + \sin\theta_1\sin\theta_2\left(\cos\varphi_1\cos\varphi_2 + \sin\varphi_1\sin\varphi_2\right), \tag{5}$$

giving

$$\cos\alpha = \cos(\theta_2-\theta_1) - 2\sin\theta_1\sin\theta_2\sin^2(\delta\varphi/2) \tag{6}$$

where $\delta\varphi=\varphi_2-\varphi_1$. Since both scattering angles θ_1 and θ_2 are small, we get

$$\alpha^2 \approx (\theta_2-\theta_1)^2 + 4\theta_2\theta_1\sin^2(\delta_\varphi/2). \tag{7}$$

If the receiving antenna is positioned for collecting with maximum efficiency the scattered waves from the first point ($\boldsymbol{k}_s^1$), those from the second point will be collected with a relative efficiency $\exp(-\alpha^2/\alpha_0^2)$, with $\alpha_0 = 2/k_i a$ [17,18]. From this and equation (7), we get the instrumental selectivity function

$$F = \exp\left[-\left((k'-k)^2 + 4k'k\sin^2(\delta_\varphi/2)\right)/\Delta^2\right], \tag{8}$$

where $\Delta = 2/a$, $k \approx k_i\theta_1$ is the tuning wave number of the scattering receiver and $k' \approx k_i\theta_2$ is the wave number of detected fluctuations. The contour plot of F as a function of position along the probing beam (s) and the wave number mismatch ($\Delta k=k'-k$) is shown in figure 4, where the angle δ_φ is from a ray tracing code using the EFIT equilibrium reconstruction code [19] and equations (3) and (4). These results show that the length of the scattering region is substantially smaller than

the above estimate of δl. In addition, because of the novel scattering geometry, the radial footprint of the scattering region is smaller than the diameter of the probing beam ($2a$), so that the radial resolution of our fluctuation measurements is ±2.5 cm together with a wave number resolution of ±1 cm^{-1}.

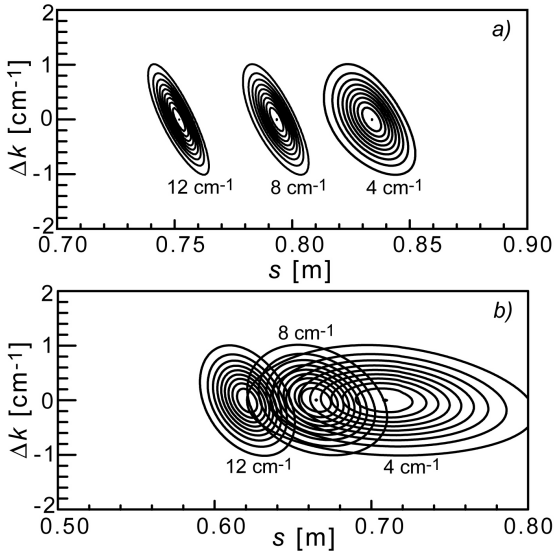

Figure 4. *Contour plot of F (ten levels equally spaced from 0.1 to 1, with maximum at Δk=0) as a function of position along the probe beam (s) and Δk=k'-k for the two scattering configurations of figure 2 ((a) inboard fluctuations, (b) outboard fluctuations). Labels are values of k.*

3. Results

The experimental results presented in this paper were obtained in plasmas with high harmonic fast wave (HHFW) heating [20]. Use of this radio frequency (RF) technique – where a wave having the frequency (30 MHz) of an ion cyclotron harmonic (~10th) is absorbed by the electrons – was motivated by its ability to produce electron temperature (T_e) profiles with large central values and steep gradients. An example is illustrated in figures 5 and 6, showing the case of a Helium discharge with a minor radius of 0.65 m, a major radius of 0.85 m, an elongation of 2, a toroidal magnetic field of 0.55 T, a plasma current of 700 kA and an RF heating power of 1.2 MW. Use of the maximum available magnetic field and low plasma current was motivated by the need to minimize the spurious effects of MHD turbulence. In addition, because of the low plasma density, i.e, a weak electron-ion coupling, the ion temperature (T_i) remained nearly constant (with central values of 0.8-1.0 keV).

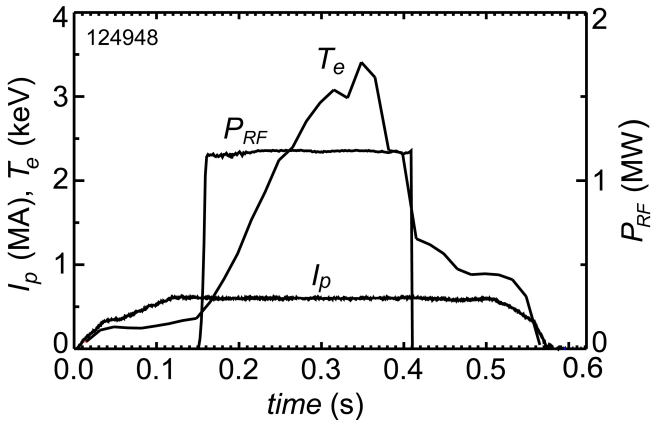

Figure 5. *Time evolution of plasma current (I_p), RF power (P_{RF}) and peak electron temperature (T_e).*

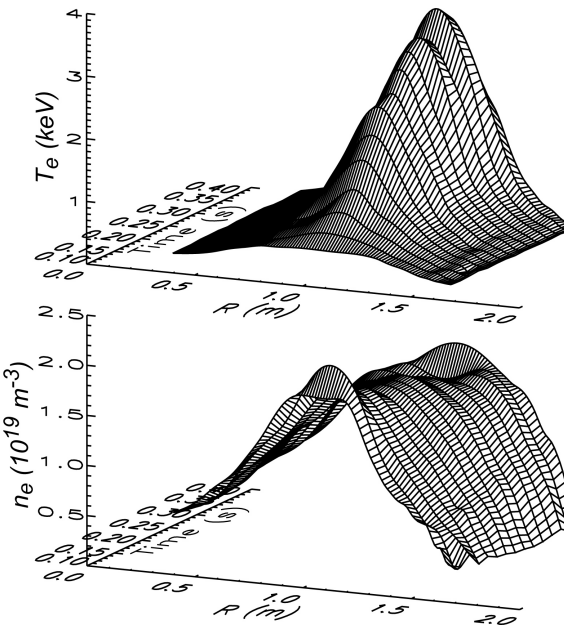

Figure 6. *Radial profiles of electron temperature T_e (top) and density n_e (bottom) in plasmas with 1.2 MW of HHFW heating.*

Figure 7 shows the time evolution of the spectral density of fluctuations with $k_\perp$= 14 cm^{-1} at r/a=0.3 (R =1.2 m), corresponding to the range of $k_\perp\rho_e$=0.2-0.4 (with ρ_e the electron gyro-radius), $k_\perp\rho_s$=8.5-17 (with ρ_s the ion gyro-radius at the electron temperature) and $k_\perp\rho_i$=8-10 (with ρ_i the ion gyro-radius). The latter implies that the source of observed fluctuations is not the Ion Temperature Gradient (ITG) mode, which is instead characterized by $k_\perp\rho_i$ <1 [1-3]. This mode is also excluded by the frequency asymmetry of measured spectra, as shown in figure 7, indicating that fluctuations propagate in the electron diamagnetic direction.

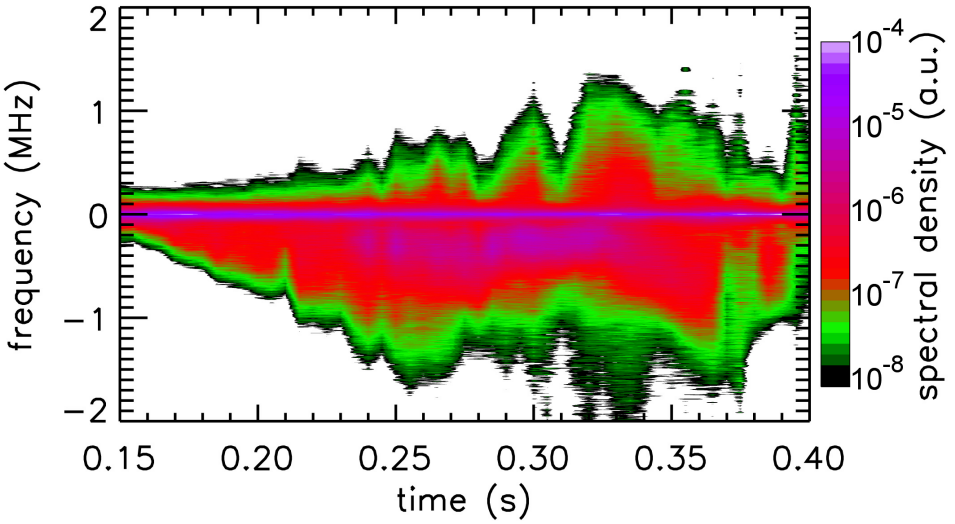

***Figure** 7. Logarithmic contour plot of the spectral density of fluctuations with $k_\perp\rho_e$=0.2-0.4 at r/a=0.3. Negative frequencies correspond to phase propagation in the electron diamagnetic direction.*

It is interesting to note that for the plasma density in figure 6, $k_\perp\delta_{sk} \sim 2$, where δ_{sk} is the collisionless skin depth ($c/\omega_{pe} = \rho_e/\beta_e^{1/2}$), with ω_{pe} the plasma frequency and β_e the electron beta). This is not surprising since for sufficiently large values of β_e, such as those in the present experiment (3-6%), the characteristic turbulence scale length is expected to be of the order of the electron skin depth [4, 21].

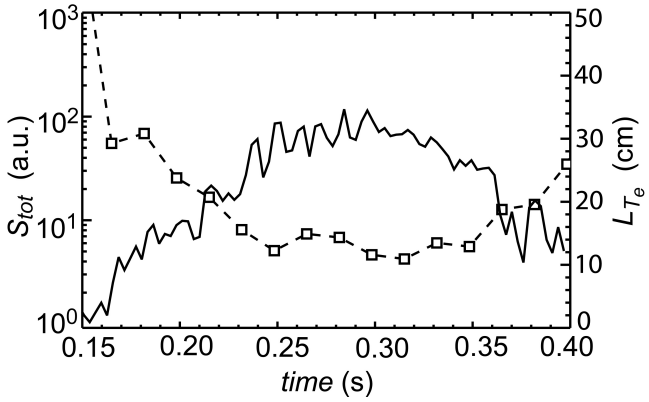

***Figure 8**. Frequency integrated spectral density S_{tot} (solid line) and radial scale L_{T_e} (dash line) for the case of figure 7.*

These turbulent fluctuations appear to be related to the electron temperature gradient, as illustrated in figure 8 where the frequency integrated value of the spectral density (S_{tot}) is compared with the electron temperature scale length (defined as L_{T_e}=(dlnT_e/dr)$^{-1}$) at the location of measurement. Note that plasma fluctuations begin to rise at the beginning of the RF pulse, when the value of L_{T_e} begins to drop, and decrease towards the end of the pulse, when the opposite occurs.

The same phenomenon is illustrated in figure 9, showing the electron temperature profile and the spectrum of measured fluctuations at

two different times, the first when the amplitude of fluctuations is maximum (0.3 s), the second 30 ms after the RF pulse (0.43 s) when the profile of T_e has collapsed and flattened on a wide central region. At the location of measurement (blue stripe in figure 9), the two cases differ only in the value of L_{Te} – i.e., temperature and density are the same – that in the first case is more than three times smaller than in the second. Correspondingly, while both spectra contain a central narrow symmetric feature (caused by a spurious stray radiation), that at 0.3 s displays a strong Doppler shifted component that is that of the scattering signal from large plasma fluctuations. This demonstrates very clearly the dependence of the measured turbulence on the radial scale of T_e.

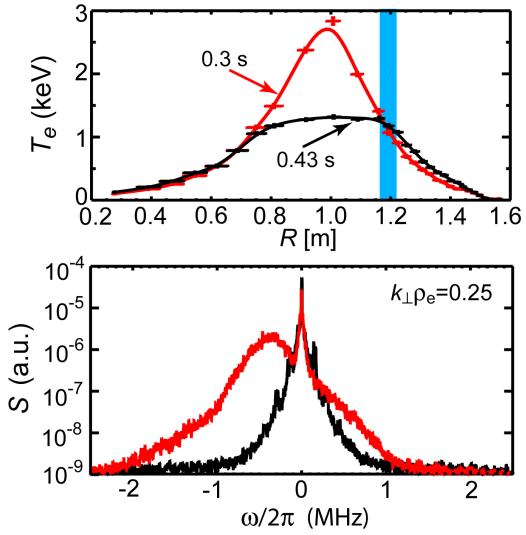

Figure 9. *Temperature profiles (top) and spectral density of fluctuations (bottom) at 0.3 (red) and 0.43 s (black). Blue stripe indicates the location of measurement where L_{Te} is 15 and 50 cm, respectively. Negative frequencies (bottom) correspond to wave propagation in the electron diamagnetic direction.*

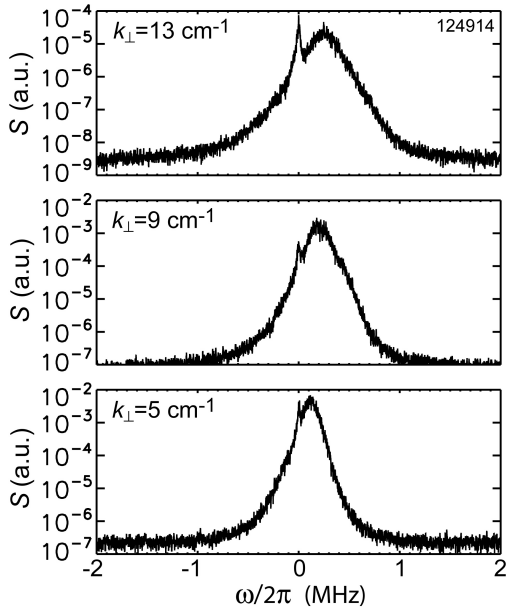

Figure 10. *Spectral density of fluctuations in the range of wave numbers $k_\perp\rho_e$=0.1-0.2 at r/a=0.6. Positive frequencies correspond to phase propagation in the electron diamagnetic direction.*

Short scale turbulent fluctuations were also detected on the outer region of the plasma column (r/a=0.6), as illustrated in figure 10 showing the spectral density of fluctuations with wave numbers in the range $k_\perp\rho_e$ =0.1-0.2 and $k_\perp\rho_i \approx k_\perp\rho_s$ = 4-8. Again, the scale length is of the order of the collisionless skin depth ($k_\perp\delta_{sk}$=1-2). As in the case of core fluctuations, wave numbers are outside the range of the ITG mode, and the phase propagation is in the electron diamagnetic direction (corresponding to positive frequencies for the scattering geometry of these measurements).

The propagation of fluctuations along the electron diamagnetic direction is of crucial importance since it rules out the ITG instability as the source of turbulence. So far in the present paper, the phase propagation of fluctuations was inferred from the sign of measured frequencies when Doppler shifts from a toroidal plasma rotation were negligible, i.e., from the sign of ω_s-ω_i together with the component of $\boldsymbol{k}$ in the diamagnetic direction. Indeed, a Doppler shift from plasma rotation could provide further evidence on the direction of wave propagation. To show this, let us consider the orthogonal system of coordinates (θ,φ,ψ) in figure 11, where the unit

vector $\boldsymbol{e}_\psi$ is in the outward normal direction to the magnetic surface (i.e., $\nabla p \cdot \boldsymbol{e}_\psi < 0$), and $\boldsymbol{e}_\varphi$ is parallel to the toroidal plasma current (i.e., $B_\theta > 0$). Let us then refer to fluctuations that in the plasma frame propagate along the electron diamagnetic velocity ($\boldsymbol{v}_{De} \equiv \Delta p_e \times \boldsymbol{B}/en_eB^2$) as electron waves and those propagating along the ion diamagnetic velocity ($\boldsymbol{v}_{Di} \equiv -\Delta p_i \times \boldsymbol{B}/en_eB^2$) as ion waves. From the equations

$$\boldsymbol{v}_{De} \cdot e_\varphi = -\frac{|\nabla p_e|B}{en_eB^2} < 0, \qquad \boldsymbol{v}_{Di} \cdot e_\varphi = \frac{|\nabla p_i|B}{en_iB^2} > 0, \tag{9}$$

one gets that a plasma co-rotation (i.e., along the plasma current) causes a frequency Doppler shift that for an ion wave has the sign of the wave frequency in the plasma frame, while for an electron wave it is the opposite. A counter-rotation has the reverse effect, i.e., the Doppler shift has the sign of the wave frequency in the plasma frame for an electron wave, and its opposite for an ion wave. Figures 12 and 13, displaying the time evolution of the spectrum of fluctuations and of the plasma velocity (driven by the neutral beam used for measurement of the plasma velocity itself), show that the frequency of measured fluctuations follows the toroidal velocity as prescribed by the first of equations (9), while it is not consistent with the second since the measured frequency increases when it should decrease and decreases when it

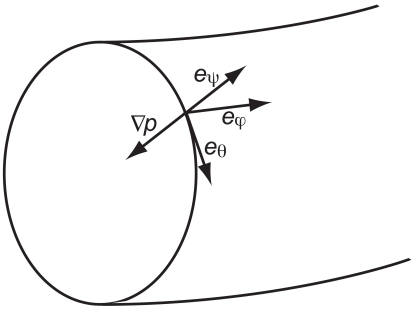

Figure 11. *Orthogonal coordinate system (θ,φ,ψ) with $\boldsymbol{e}_\psi$ along the outward normal to the magnetic surface and $\boldsymbol{e}_\varphi$ parallel to the toroidal plasma current.*

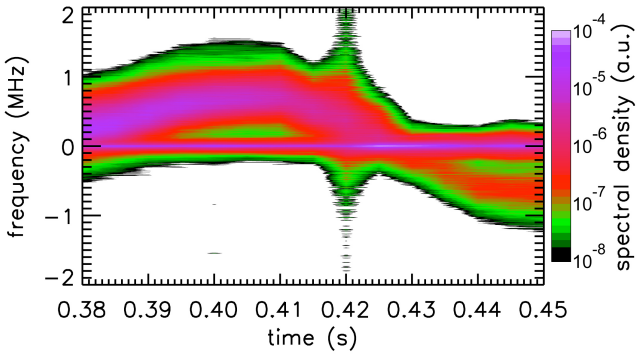

Figure 12. *Time evolution of the spectrum of fluctuations with $k_\perp$=13 cm^{-1} for the plasma rotation of figure 13 (burst at 0.42 s was caused by the abrupt termination of the RF pulse by the onset of an MHD instability).*

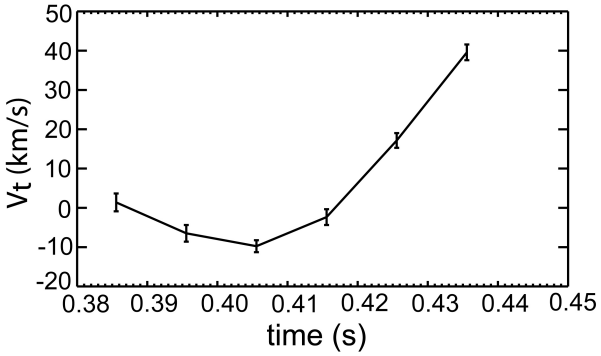

Figure 13. *Time evolution of the toroidal plasma velocity (positive when along the plasma current).*

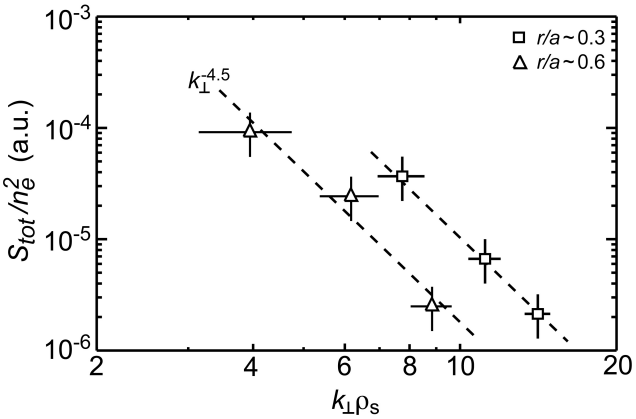

Figure 14. *Power spectrum of fluctuations (normalized to n_e^2) as a function of $k_\perp$ for both inboard (squares) and outboard (triangles) measurements.*

should increase. Hence the conclusion that measured fluctuations propagate in the electron diamagnetic direction.

Finally, the power spectrum of measured fluctuations (i.e., the value of S_{tot} normalized to n_e^2 at 0.3 s) is shown in figure 14 as a function of $k_\perp$ for both inboard (figure 7) and outboard (figure 10) measurements. Surprisingly, the power spectrum follows a similar power law ($\sim k_\perp^{-4.5}$) at both plasma locations in spite of a different value of T_e (1.5 vs. 0.5 keV). If the measured fluctuations were isotropic perpendicularly to $\boldsymbol{B}$ – a fact that our measurements could not prove – the mean square density fluctuation would follow the power law $\left\langle \left| \tilde{n}_e^2 \right| \right\rangle / n_e^2 \propto k_\perp^{-3.5}$.

4. ETG Critical Gradient

In an attempt to determine the source of observed fluctuations, we employed a linear version of the GS2 stability code [22] to obtain the normalized critical gradient $(R/L_{Te})_{crit}$ for the onset of the ETG instability. This code solves the gyrokinetic Vlasov-Maxwell equations, including passing and trapped particles, electromagnetic effects, as well as a Lorentz collision operator. The results are shown in figure 15, where the critical gradient is compared with the measured normalized temperature gradient R/L_{Te} for the case of figure 7. From this, we conclude that the ETG mode is indeed unstable over most of the RF pulse where the critical gradient is smaller than the electron temperature gradient. A comparison with S_{tot} in figure 7 shows that the level of measured fluctuations correlates with the departure of the temperature gradient from the critical gradient.

Figure 15 displays also an algebraic expression of the normalized critical gradient that was derived in [23] using a best fit of GS2 results for a set of model tokamak configurations [23]. This is given by

$$(R/L_{Te})_{crit}=(1+Z_{eff}T_e/T_i)(1.3+1.9s/q)(1-1.5\varepsilon), \qquad (10)$$

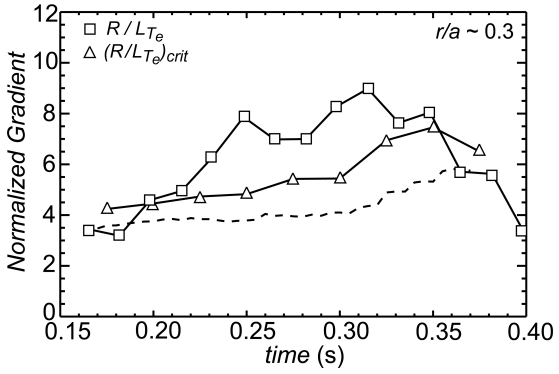

Figure 15. *Time evolution of measured gradient R/L_{Te} (squares) and GS2 critical gradient $(R/L_{Te})_{crit}$ (triangles) for the onset of the ETG mode in the case of figure 7. Dash line is the critical gradient from [23].*

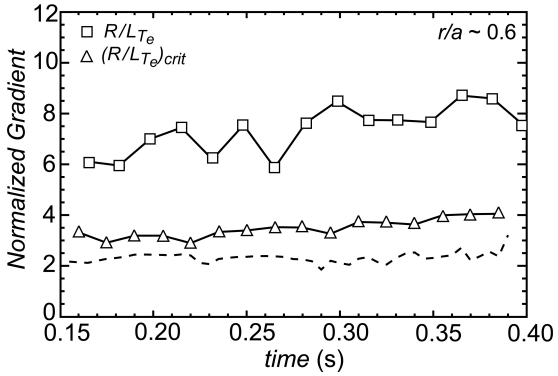

Figure 16*. Same as in figure 15 for the case of figure 10.*

where Z_{eff} is the ionic effective charge (~2.5 in figure 15), $s = r(d\ln q/dr)$ is the magnetic shear and $\varepsilon=r/R$ is the inverse aspect ratio. This formula, showing the stabilizing role of the temperature ratio T_e/T_i and the magnetic shear, gives values of critical gradient that are not very

different from those obtained from the GS2 code using the exact plasma configuration of our experiment.

Similar plots are displayed in figure 16 for the case of outboard fluctuations (figure 9), showing again that fluctuations coincide with a temperature gradient larger than the critical gradient. At this plasma location, however, since the HHFW heating did not modify significantly plasma conditions, both the amplitude of measured fluctuations and the ETG critical gradient remained nearly constant in time.

5. Negative Magnetic Shear

It is known that a negative magnetic shear can induce – under certain conditions – the formation of an internal transport barrier (ITB), resulting in drastically reduced outflow of plasma energy. The signature of an electron ITB is a sharp temperature gradient at the barrier location, inside which the profile of T_e is nearly flat. If the turbulent fluctuations described in this paper are the cause – even if partially – of the electron anomalous transport in tokamaks, they should be suppressed at the location of an electron ITB.

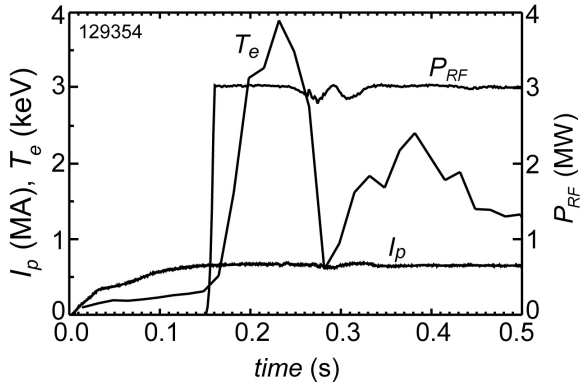

***Figure 17**. Time evolution of plasma current (I_p), RF power (P_{RF}) and peak electron temperature (T_e) in a plasma with negative magnetic shear.*

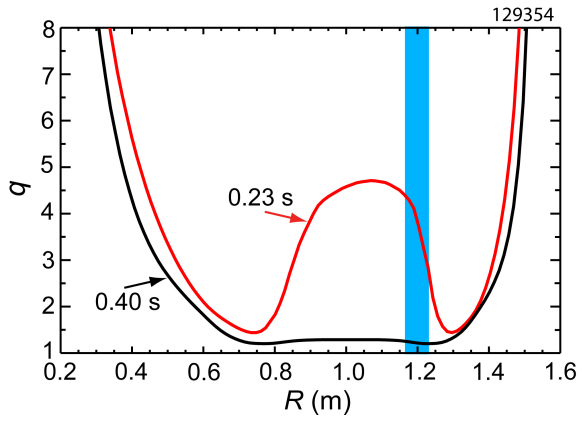

***Figure 18**. Magnetic safety factor on the equatorial plane at the peak of T_e (red) and after the collapse of negative magnetic shear (black). Blue stripe indicates the location of fluctuation measurements.*

A simple procedure for producing NSTX plasmas with negative magnetic shear is to launch a high power HHFW pulse early in the discharge, when the toroidal current is still diffusing from the plasma edge to the center. An example is shown in figure 17, where 3 MW of HHFW heating are launched into a Deuterium plasma at 0.15 s. A strong electron heating together with a low Z_{eff} (~1.4) has the effect of slowing down the diffusion of plasma current and forming a central region with strong negative magnetic shear (figure 18), lasting until the onset of an MHD instability causes a fast redistribution of the plasma current and a flattening of its radial profile. During the phase of negative shear, the electron temperature develops a steep gradient near the radius of minimum q (figure 19) that indicates the presence of an ITB. Figures 20 and 21 show that indeed fluctuations are suppressed at the transport barrier – a striking similarity to what was found previously in similar TFTR plasmas [24], albeit for fluctuations driven by the ion temperature

gradient (ITG). However, turbulent fluctuations reappear (figures 21) as soon as the plasma current diffuses to the plasma core, making the q-profile nearly constant over a wide central region (figure 18).

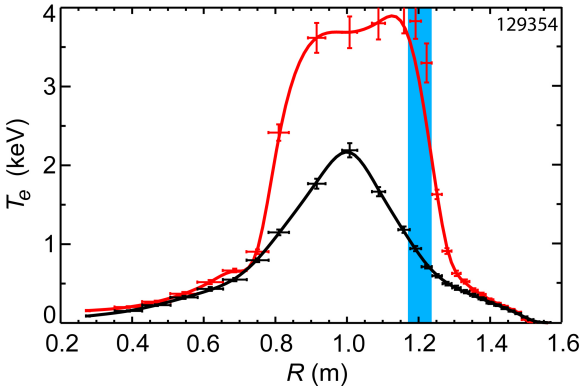

Figure 19. *Same as in figure 18 for T_e.*

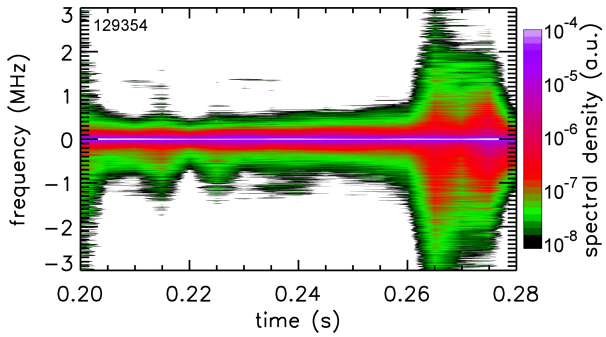

Figure 20. *Spectral density of measured fluctuations (same scattering geometry as in figure 7) during negative reversed shear. The sudden rise at t=0.26 coincides with the collapse of the ITB.*

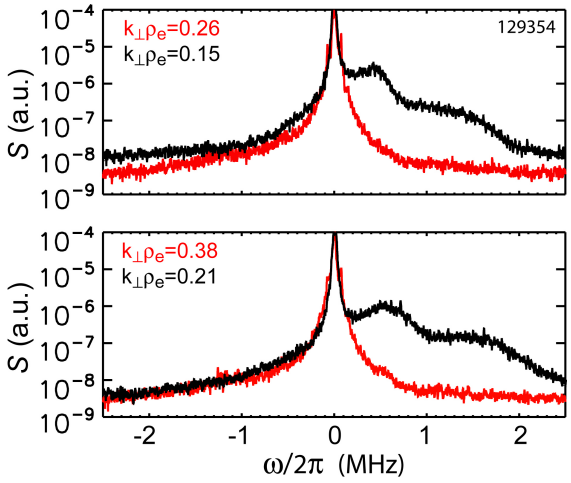

Figure 21. *Same as in figure 18 for the spectrum of fluctuations.*

5. Conclusion

In conclusion, turbulent fluctuations have been observed in NSTX plasmas in the range of wave numbers $k_\perp\rho_e$= 0.1-0.4, corresponding to a radial scale of the order of the collisionless skin depth. Large values of $k_\perp\rho_i$, a strong correlation with the scale of T_e and phase propagation in the electron diamagnetic direction exclude the ITG mode as the source of turbulence. Experimental observations and agreement with numerical results from the linear gyrokinetic GS2 code support the conjecture that the observed turbulence is driven by the electron temperature gradient.

These fluctuations were not observed at the location of an internal transport barrier driven by a strong negative magnetic shear. Even though this could be used as evidence of the role played by measured fluctuations on plasma transport, additional experiments together with nonlinear

numerical simulations of plasma turbulence are needed before reaching any definite conclusion on the importance of observed fluctuations.

This work was supported by U. S. Department of Energy Contract No. DE-AC02-76CH03073 and Grant No. DE-FG-02-99ER54518.

References

[1] B. Coppi and G. Rewoldt, in *Advances in Plasma Physics,* edited by A. Simon and W. B. Thompson (John Wiley and Sons, New York, 1976), Vol. 6, p. 421.

[2] W. Horton, Rev. Mod. Phys. **71**, 735 (1999).

[3] J. W. Connor and H. R. Wilson, Plasma Phys Control. Fusion **36,** 719 (1994).

[4] W. Horton, P. Zhu, G. T. Hoang, T. Aniel and X. Garbet, Phys. Plasmas **7**, 1494 (2000).

[5] W. Dorland, F. Jenko, M. Kotschereuther and B. N. Rotgers, Phys. Rev. Lett. **85**, 5579 (2000).

[6] F. Jenko and W. Dorland, Phys. Rev. Lett. **89**, 225001 (2002).

[7] W. M. Nevins, J. Candy, S. Cowley, T. Dannert, A. Dimits, W. Dorland, C. Estrada-Mila, G. W. Hammett, F. Jenko, M. J. Pueschel and D. E. Shumaker, Phys. Plasmas **13**, 122306 (2006).

[8] A. M. Dimits, W. N. Nevins, D. E. Shumaker, G. W. Hammett, T. Dannert, F. Jenko, M. J. Pueschel, W. Dorland, S. C. Cowley, J. N. Leboeuf, T. L. Rhodes, J. Candy and C. Estrada-Mila, Nucl. Fusion **47**, 817 (2007).

[9] R. E. Waltz, J. Candy, and M. Fahey, Phys. Plasma **14**, 0561116 (2007).

[10] W. Horton, G. T. Hoang, C. Bourdelle, X. Garbet, M. Ottaviani and L. Colas, Phys. Plasmas **11**, 2600 (2004).

[11] A. D. Gurchenko, E. Z. Gusakov, A. B. Altukhov, A. Yu. Stepanov, L. A. Esipov, M. Yu. Kantor, D. V. Kouprienko, V. V. Dyachenko and S. I. Lashkul, Nucl. Fusion **47**, 245 (2007).

[12] S. M. Kaye, R.E. Bell, D. Gates, B. P. LeBlanc, F. M. Levinton, J.E. Menard, D. Mueller, G. Rewoldt, S.A. Sabbagh, W. Wang and H. Yuh, Phys. Rev. Lett. **98**, 175002 (2007).

[13] E. Mazzucato, D. R. Smith, R. E. Bell, S. M. Kaye, J. C. Hosea, B. P. LeBlanc, J. R. Wilson, P. M. Ryan, C. W. Domier, N. C. Luhmann, Jr., H. Yuh, W. Lee and H. Park, Phys. Rev. Lett. **101**, 075001 (2008).

[14] E. Mazzucato, Phys. Rev. Lett. 36, 792 (1976).

[15] M. N. Rosenbluth and N. Rostoker, Phys. Fluids **5**, 776 (1962).

[16] D.R. Smith, E. Mazzucato, W. Lee, H. Park, W. Domier and N. C. Luhmann, Jr., to be published in Rev. Sci. Instrum.

[17] E. Mazzucato, Phys. Plasmas **10**, 753 (2003).

[18] E. Mazzucato, Plasma Phys Control. Fusion **48,** 1749 (2006).

[19] L. L. Lao, H. St. John, R. D. Stambaugh, A. G. Kellman and W. Pfeiffer, Nucl. Fusion **25**, 1611 (1985).

[20] J. Hosea, R. E. Bell, B. P. LeBlanc, C. K. Phillips, G. Taylor, E. Valeo, J. R. Wilson, E. F. Jaeger, P. M. Ryan, J. Wilgen, H. Yuh, F. Levinton, S. Sabbagh, K. Tritz, J. Parker, P. T. Bonoli and R. Harvey, Phys. Plasmas **15**, 056104 (2008).

[21] B. Coppi, in *Collective Phenomena in Macroscopic Systems*, edited by G. Bertin (World Scientific, Singapore, 2007).

[22] M. Kotschenreuther, G. Rewoldt, and W. M. Tang, Comput. Phys. Commun. **88**, 128 (1995).

[23] F. Jenko, W. Dorland and G. W. Hammett, Phys. Plasmas **8**, 4096 (2001).

[24] E. Mazzucato, S. H. Batha, M. Beer, M. Bell, R. E. Bell, R. V. Budny, C. Bush, T. S. Hahm, G. W. Hammett, F. M. Levinton, R. Nazikian, H. Park, G. Rewoldt, G. L. Schmidt, E. J. Synakowski, W. M. Tang, G. Taylor and M. C. Zarnstorff, Phys. Rev. Lett., **77**, 3145 (1996).